Plasma Etching Durability of Poly(methyl Methacrylate)

KATSUHIRO HARADA, *Nippon Telegraph and Telephone Public Corporation, Ibaraki Electrical Communication Laboratory, Tokai, Ibaraki, 319-11, Japan*

Synopsis

The decomposition of poly(methyl methacrylate) (PMMA), as a positive resist, in CF_4/O_2 plasma etching has been studied in the thin film state in order to clarify the factors influencing the dry etching durability of resists. It becomes clear that the major PMMA decomposition in CF_4/O_2 plasma etching proceeds by the mechanism of random chain scission because very small kinetic chain lengths are estimated from the gel permeation chromatography data. The Arrhenius plots for the plasma etching rate of PMMA bend above about the glass transition temperature (T_g), where rapid increase of the etching rate and remarkable pattern deformation are observed. Activation energy of the PMMA etching rate which is changed by oxygen concentration and rf power indicates various values from 3.1 to 6.5 kcal/mole below about T_g. The result of molecular weight variation in the cross section of the film suggests that the active species permeate into the film with fairly large speed and the PMMA decomposition occurs not only at the film surface but also at deep layer of the film.

INTRODUCTION

Dry etching such as plasma etching, reactive ion etching, and ion-beam etching are excellent techniques for fabricating electronic devices with very fine dimensions. The resist materials used in the dry etching process must have high durability, in addition to high sensitivity and high resolution in the lithographies using electron beams and x rays.

It is well-known that the positive resist has superior resolution even in submicron dimension, however, its dry etching durability tends to conflict with the sensitivity. As one of the approaches to the subject, the author reported that the positive resist durability is improved by additives such as radical scavengers and plastics anti-oxidants without reducing the sensitivity to the electron beam.[1] However, in order to achieve a highly durable resist that realizes the dry process with more fine dimension and precision, both approaches of developing the resist material and deriving the optimum etching conditions are necessary.

Dry etching, especially plasma etching, has been studied in detail[2,3] concerning active species, etching mechanism, etching rate, etc., with respect to various conditions for many kinds of substrate. But the effects on resist durability under various conditions have been scarcely studied. A dry etching atmosphere seems chemically very complex, because, in many active species such as radicals, ions and many other excited species and significant amounts of atomic oxygen exist at relatively high gas temperature. Positive resists could be liable to decompose or denature under such conditions.

The object of this paper is to clarify the factors that influence the resist durability.

Journal of Applied Polymer Science, Vol. 26, 1961–1973 (1981)
 CCC 0021-8995/81/061961-13$01.30

EXPERIMENTAL

Materials

Poly(methyl methacrylate)(PMMA) is a well-known electron beam resist and probably one of the more widely used positive resists. PMMA was used here as the model positive resist.

The molecular weight of PMMAs are shown in Table I. PMMA-2 is commercially available Elvacite 2041 (du Pont). Other PMMAs were prepared by ordinary radical polymerization technique. PMMA-2 was used mainly except for the cases indicated.

PMMA films in various thicknesses were prepared on thermally oxidized silicon wafer using the standard spin-coating technique, then they were baked in air for 30 min at 170°C before plasma etching and electron beam exposure in order to release the spining solvent. It was confirmed by gel permeation chromatography (GPC) measurement that such a heat treatment did not decompose the PMMA.

Plasma Etching

Plasma etching is the selective etching of materials by the reaction with chemically active species formed in a glow discharge. Generally, using ordinary plasma etching apparatus, the temperature of etching atmosphere rises with time gradually, therefore, the etching rates both of resist and substrate are accelerated and those relationships between etching depth and time indicate an accelerated curve.

The most inconvenient fact is that the etching rate is influenced by the environmental temperature. The improved etching apparatus shown in Figure 1 was used in the current work. The main body was a commercially available tunnel reactor IPC-2005 (International Plasma Corp.) on which was impressed 13.56-MHz rf power. A glass sample stage in which a heat medium was circulated was applied additionally to the main body. The heat medium was controlled at a given temperature by the thermostat.

During etching, the temperatures of PMMA coated wafers were controlled by contact with the sample stage.

PMMA and SiO_2 etching depth with time shown in Figures 2 and 3 indicate linear relationships pássing through the origin using the improved apparatus. The results mean that the sample was maintained at a constant temperature during etching. The temperature of the heat medium and the slope of the line are defined here as the etching temperature and the etching rate, respectively.

The PMMA durability for plasma etching was estimated by the etching rate of PMMA, that is, the low etching rate shows high durability and vice versa.

TABLE I
Molecular Weight of PMMAs

Sample name	$\overline{M}_n$	$\overline{M}_w$	$\overline{M}_w/\overline{M}_n$	Remarks
PMMA-1	1.0×10^4	1.9×10^4	1.9	
PMMA-2	1.3×10^4	3.7×10^4	2.8	Elvacite-2041
PMMA-3	1.9×10^5	6.1×10^5	3.2	
PMMA-4	1.5×10^6	4.0×10^6	2.6	

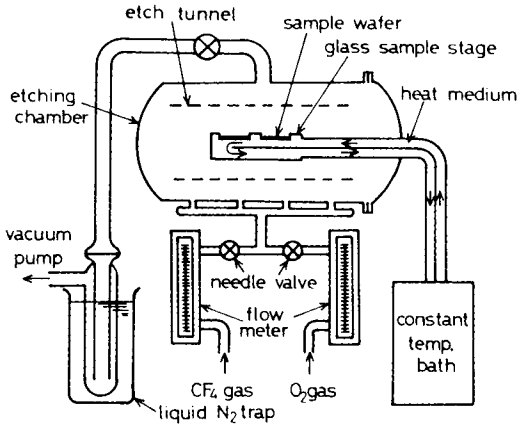

Fig. 1. Schematic diagram of the experimental apparatus.

All etching processes were performed at the constant loading effect using a perforated shield or an etch tunnel made by aluminum. The total gas flowrate was kept at 100 cm^3/min for all etching processes. The feed gas composition was decided by the flowrate ratio of O_2 to CF_4. The gas pressure was 0.7–0.8 Torr for below 5% O_2 and 0.8–1.1 Torr above 5% O_2.

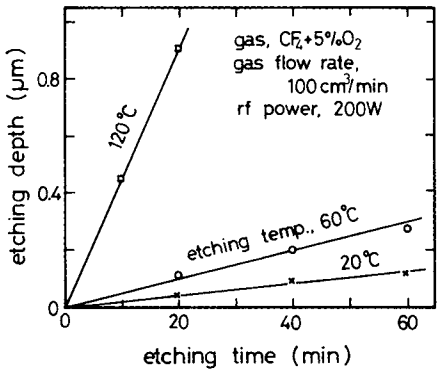

Fig. 2. Typical etching characteristics of PMMA.

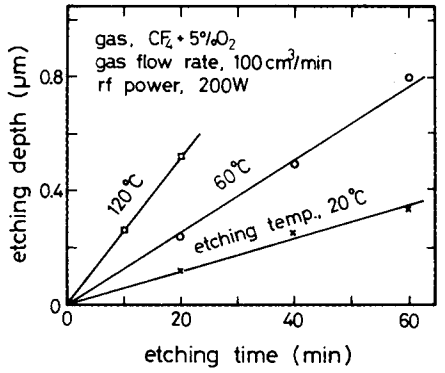

Fig. 3. Typical etching characteristics of SiO_2.

PMMA thicknesses before etching were adjusted from 0.6 μm for low etching rates to 3.0 μm for large etching rates in order to attain a high precision of measurements. Variations of the etching rates with initial thicknesses were scarcely observed.

The etching depths of PMMA and SiO_2 were measured by a Talystep (Taylor-Hobson).

Measurement of GPC

The molecular weights and its distributions of PMMA and plasma etched PMMA were measured by a GPC (HLC-802UR, Toyo Soda Kogyo) using tetrahydrofuran solvent.

Small molecular weight fractions below 1×10^3, which were contained in plasma etched PMMAs, were excluded from $\overline{M}_w$ and $\overline{M}_n$ calculations for some technical reasons of the measurement.

RESULTS AND DISCUSSION

Mechanism of PMMA Decomposition in CF_4/O_2 Plasma Etching

The etching rates of PMMAs with different molecular weights and molecular weight variations with etching time were examined in order to estimate the PMMA decomposition mechanism in the plasma etching.

The decomposition mechanism of PMMA has been widely studied in the gamma radiolysis,[4] photolysis,[5] and thermal decomposition.[6] The mechanism is different in those processes and treatment temperature, e.g., random scission for photodegradation below the glass transition temperature (T_g),[7] depropagation mechanism above T_g,[5] and end-initiated depropagation for thermal decomposition.[6]

The plasma etching condition seems to be very complex to analyze the polymer decomposition induced by it, because many kinds of active species and significant amounts of oxygen exist in it with relatively high gas temperature. Oxygen is usually added to CF_4 etching gas in order to increase the etching rates of Si and SiO_2.

Many kinds of active species have been assigned or detected,[8,9] in CF_4/O_2 plasma, such as radicals (e.g., CF_3, CF_2, CF), atoms (e.g., F, O) and ions (e.g., CF_3^+, CF_3^-, F^-). Such atomic oxygen and radicals could possess a remarkable ability to decompose a polymer in distinct ways.

The PMMA decomposition in CF_4/O_2 plasma therefore is postulated to take place by the following three steps, and each step may be described as the competitive reaction among some reactions as follows.

Initiation:

- (R1) random chain scission, decomposition of side group, and chain-end initiation;
- (R2) reaction of polymer with plasma induced atomic oxygen;
- (R3) reaction of polymer with plasma induced radicals;

Propagation:

- (R4) depropagation and transfer;
- (R5) reaction of polymer with atomic oxygen;
- (R6) reaction of polymer radicals with oxygen;

Termination:

(R7) first order and second order.

R1 contains a well-known reactions for PMMA decomposition. These reactions are induced by the absorption of energies such as electron, photon, and heat.

Battey[10] has reported that the stripping rate of photoresist (Waycoat) is proportional to the flowrate of atomic oxygen induced in an oxygen plasma. However, the mechanism of polymer decomposition by atomic oxygen has scarcely been clarified. Tsuda et al.[11] has proposed the resist decomposition mechanism by atomic oxygen induced in an oxygen plasma using the theoretical calculation of the reaction coordinate. The mechanism, in which *n*-pentane is dealt with as a resist model, consists of four stages: (1) the production of an alcohol, (2) the production of a gem-diol and decomposition to C = 0 + H_2O, (3) the main chain oxidation, and (4) the formation of peroxide for the main chain cleavage. R2 and R5 also could consist of similar mechanism to above.

R3 could occur in the plasma etching; one example to cite is abstracting of secondary hydrogen by plasma induced radicals I·.

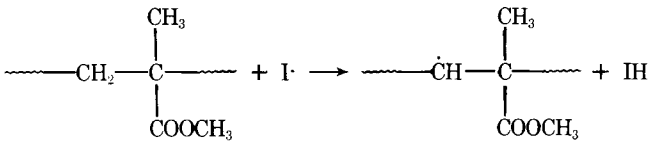

This polymer radical decomposes to give the unsaturated polymer chain end and another polymer free radical.[12]

R4 is an ordinary reaction occuring in linear degradable polymers, in particularly, the thermal PMMA decomposition *in vacuo* almost only undergoes depropagation because high monomer yield is observed.[13]

Molecular oxygen reacts easily with polymer radicals and corresponding peroxy radicals are formed for the main chain scission.[13] Similarly, PMMA is expected to react in R6.

The termination reactions which are caused by the plasma induced radicals and peroxy radicals[14] are expected additionally to the ordinally termination reactions.

Figure 4 shows the etching rates of PMMAs with different number average molecular weights $\overline{M}_n$ at the etching temperature of 60°C. There is little difference in the etching rates with $\overline{M}_n$.

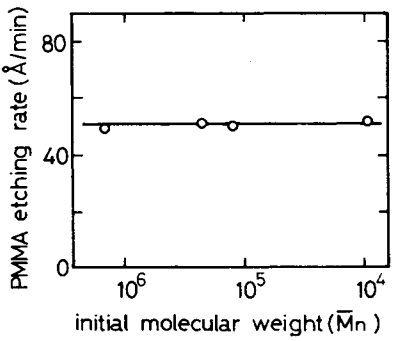

Fig. 4. Dependence of the etching rate on initial molecular weights of PMMA (etching gas, CF_4/O_2 = 95/5; etching temperature, 60°C; rf power, 200 W).

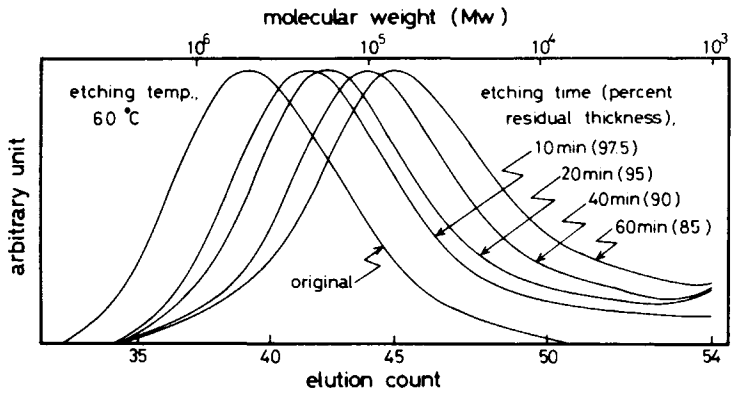

Fig. 5. GPC curves of plasma etched PMMA at 60°C (PMMA-3; etching gas; CF_4/O_2 = 95/5; rf power, 200 W; initial film thickness, 2.0 μm).

Figures 5 and 6 show GPC curves of original and plasma etched PMMAs in different etching times at the etching temperatures of 60 and 100°C. The molecular weight decreases gradually with time, and there is not a remarkable difference of tendency between two series.

Figure 7 shows the variation of $\overline{M}_n$ and $\overline{M}_w$ to percent residual thickness calculated from Figures 5 and 6. The exceptionally steep decreases of $\overline{M}_n$ are characteristic at early state of the etching.

From Figures 4 and 7, one can presume readily the decomposition mechanism that proceeds by random chain scission.

Jellinek[14] studied in detail the kinetics of polymer decomposition. He has derived the kinetic equation (1) for the degradation of monodispersed polymer, which proceeds at random initiation, depropagation, and first-order termination

$$\ln(1-c) = 2\bar{\epsilon}k_{ir}t = \frac{2\bar{\epsilon}}{2L+1}\left\{\ln\left[\left(1-\frac{1+2L}{Dp_0}\right)-\ln\left(1-\frac{1+2L}{\overline{D}_p}\right)\right]\right\} \quad (1)$$

where c is the fractional conversion at time t, $\bar{\epsilon}$ is the number average kinetic chain length, k_{ir} is the rate constant for random scission, L is the chain length of the largest volatile chain, Dp_0 is the initial chain length, and $\overline{D}p$ is the chain length at c.

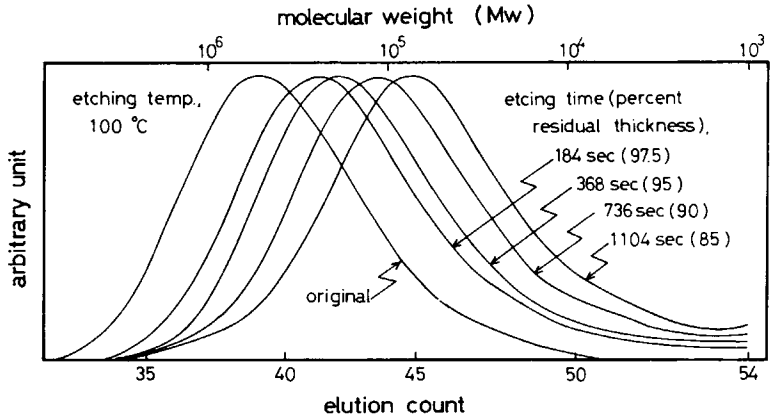

Fig. 6. GPC curves of plasma etched PMMA at 100°C (PMMA-3; etching gas, CF_4/O_2 = 95/5; rf power, 200 W; initial film thickness, 2.0 μm).

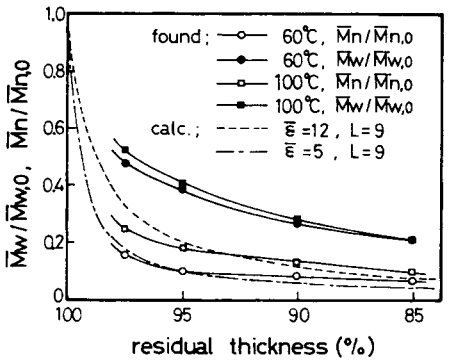

Fig. 7. PMMA decomposition curves [etching gas, CF_4/O_2 = 95/5; rf power, 200 W; initial film thickness, 2.0 μm; dotted lines are calculated by eq. (1)].

If it is assumed that $Dp_0 = \overline{M}_{no}/m$, $\overline{D}p = \overline{M}_n/m$, $c = \delta/\delta_0$, and $L = 9$, the decomposition curves are obtained for given $\bar{\epsilon}$. Where $\overline{M}_{n0}$ and $\overline{M}_n$ are the number average molecular weight for $c = 0$ and c, m is the molecular weight of monomer, δ_0 and δ are the film thickness for $c = 0$ and c, and the most large chain length which is excluded from the $\overline{M}_w$ and $\overline{M}_n$ calculations is applied to L ($L = 9$) for convenience. Even though more small L is applied, the variation of the decomposition curve is very small.

The calculated curves for $\bar{\epsilon} = 12$ and 5 are shown in Figure 7 by the dotted lines. The plasma decomposition curves of PMMA at 100 and 60°C reveal good approximation to the calculated curves for $\bar{\epsilon} = 12$ and 5, respectively. The small deviation between calculated and experimented curves are considered to be caused by the assumptions of the monodisperse polymer and the nonuniformity of decomposition rates in the cross section of the film, which will be described later.

The estimated results of fairly small $\bar{\epsilon}$ suggests that the PMMA decomposition proceeds dominantly by random chain scission. $\bar{\epsilon}$ for photolysis and thermal decomposition are from several hundreds to a thousand, which is estimated from the decomposition curves of references,[15,16] and those decompositions are characterized by the depropagation mechanism. From those large difference of $\bar{\epsilon}$, it can be considered that R2, R3, R5, and R6 contribute to random chain scission, because those reactions form random chain scission. It is also considered that $\bar{\epsilon}$ at 100°C, which is estimated somewhat large value compared to that at 60°C, indicates the increase of depropagation with the rise of etching temperature.

Temperature Effects on PMMA Plasma Etching

The temperature dependences of the PMMA etching rate are shown in Figures 8 and 9 displayed by an Arrhenius plot. The PMMA etching rates depend largely on the etching temperature, especially, the etching rates increase accelerating rapidly above 60–90°C, where the bent Arrhenius plots are obtained. It is considered that the bend of Arrhenius plots is caused by the accelerated contribution of depropagation above T_g.

It is easily accepted that a molecular mobility of polymers increases abruptly

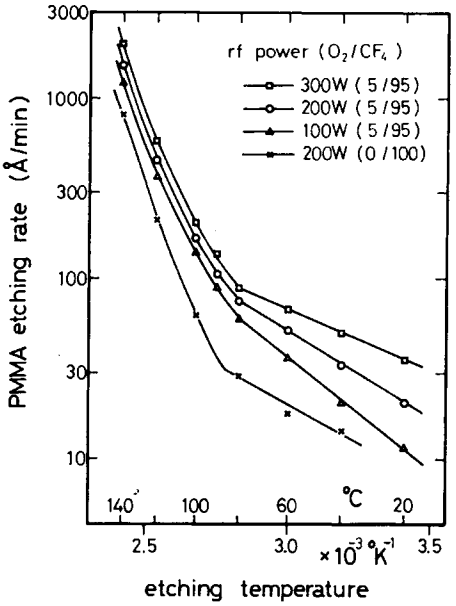

Fig. 8. PMMA etching rate as a function of temperature for some O_2 concentrations and rf powers.

above T_g and the probability of chemical reaction also increases together. There are many reports about such an enlargement of a polymer reactivity above T_g.[17,18] The rate of propagation reactions (R4, R5, and R6) could largely increase by increasing such the molecular mobility.

The surface and sectional views of plasma etched PMMA pattern at different temperatures are shown in Figure 10. Their substrates SiO_2 were etched in the same depth (0.5 μm). The PMMA pattern before etching [Fig. 10(A)], which was 1.0 μm thick, was delineated by ordinary electron beam lithography.

It is observed that a thickness loss and a pattern gap increase according to the rise of etching temperature. This seems reasonable as seen in Figures 8 and 12,

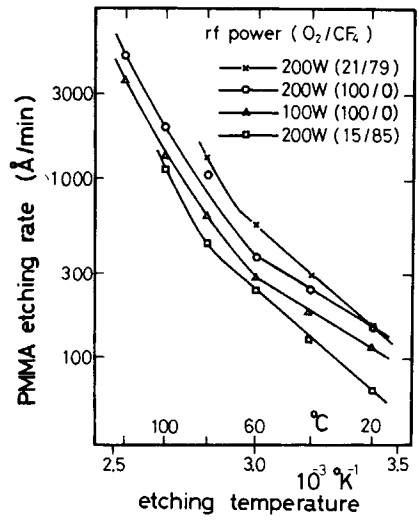

Fig. 9. PMMA etching rates as a function of temperature for some O_2 concentrations and rf powers.

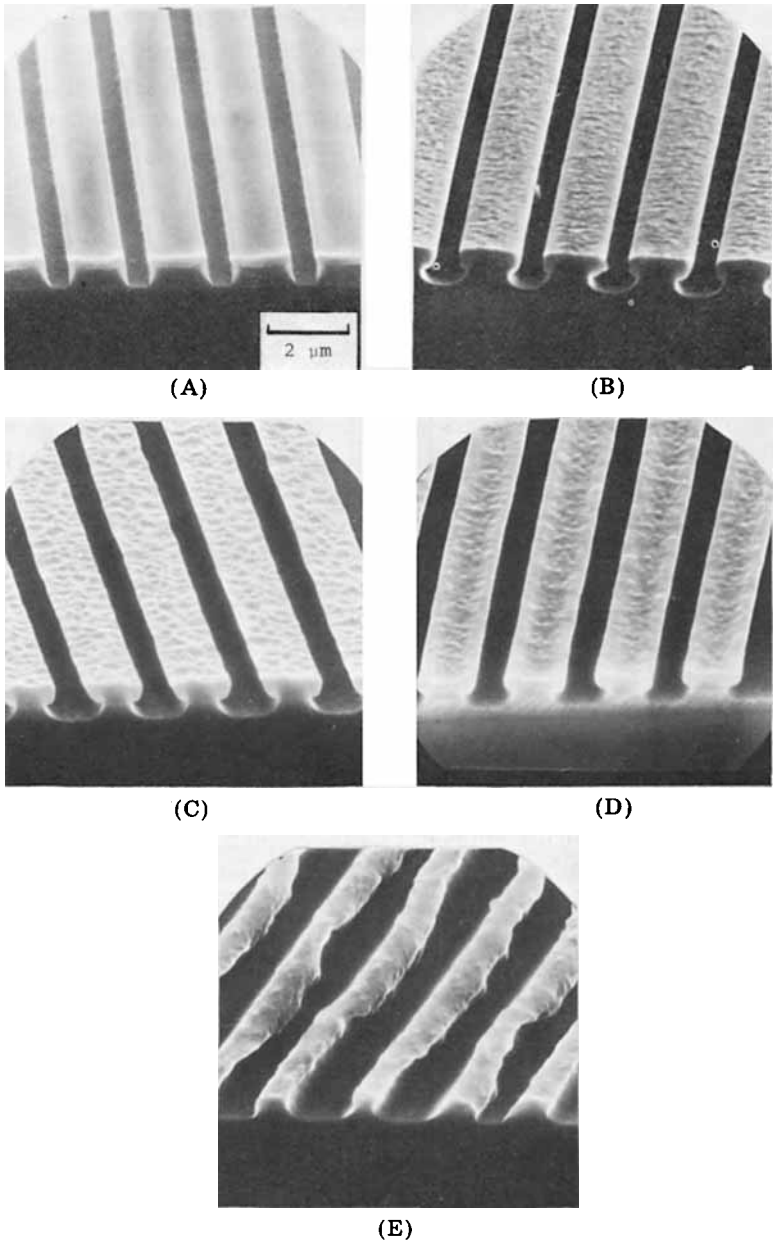

Fig. 10. Photographs of plasma etched PMMA pattern for the various etching temperatures and etching times (A) original, (B) 40°C, 56 min, (C) 60°C, 42 min, (D) 80°C, 32 min, and (E) 100°C, 27 min (gas, CF_4/O_2 = 95/5; rf power, 200 W; initial film thickness, 1.0 μm; their substrate SiO_2 are all etched about 0.5 μm).

which will be described later. The more remarkable fact observed is the pattern deformation at 100°C such as tortion and fall down, and its surface looks as it softening occurs. This result indicates that the real temperature of PMMA exceeds T_g.

PMMA has a T_g at 104°C, however, the bend of PMMA Arrhenius plots in

Figures 8 and 9 occurs at 60–90°C. The variation from 60 to 90°C seems to depend on O_2 concentration. One can anticipate that this distinction is due to both of the temperature deviation between film surface and heat medium and the increase of contribution of R5 and R6, which is caused by increasing the O_2 concentration.

It is important that, in practical plasma etching, the etching temperature is maintained below the bending point of Arrhenius plot in order to achieve the accurate process.

Effects of Oxygen Concentration on PMMA Plasma Etching

The etching rates of PMMA and SiO_2 were examined at various concentrations of O_2 in CF_4. The result is shown in Figure 11.

The PMMA etching rate changes largely with O_2 concentration compared with the SiO_2 etching rate. The most important thing to note about Figure 11 is that these respective maxima exist at quite distinct O_2 concentrations.

Mogab et al.[19] has suggested that a fluorine atom is a major etchant for SiO_2 in CF_4/O_2 discharge. Thus, the result in Figure 11 suggests the existence of other active species that cause the PMMA decomposition except for the fluorine atom. This active species must be atomic oxygen.

Figure 12 shows the Arrhenius plots of the SiO_2 etching rates for different rf powers and O_2 concentrations. All the Arrhenius plots reveal almost the same slope (activation energy, 2.9 kcal/mole), and these results indicate diffusion control. The Arrhenius plots of the PMMA etching rate give various slopes with respect to rf power, O_2 concentration, and etching temperature, shown in Figures 8 and 9.

Activation energies calculated from Figures 8 and 9 are from 3.1 to 6.5 kcal/mole in the linear region below 60–90°C, shown in Table II. The largest and smallest activation energies above 60–90°C at 27 and 9.7 kcal/mole obtained from 100% CF_4 and 100% O_2 plasma, respectively. Magnitude of the largest activation energy suggests chemical control, in which R1, R3, and R4 must contribute to the PMMA decomposition. Relatively small magnitude of activation energies,

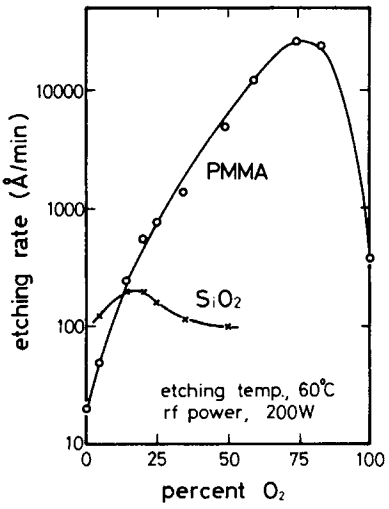

Fig. 11. Dependence of the etching rate on O_2 concentration in CF_4.

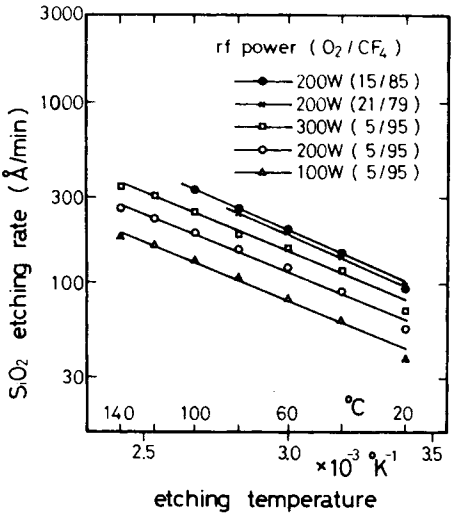

Fig. 12. SiO_2 etching rates as a function of the etching temperature for some O_2 concentrations.

which are obtained at the etching temperatures below 60–90°C, and the large O_2 concentration suggest diffusion control. Activation energy is changed by rf power, even if the etching is undergone in the same O_2 concentration, as shown in Table II. The amount of atomic oxygen must increase according to increasing rf power. The production of atomic oxygen could reach maximum at about 75% O_2 in the same rf power shown in Figure 11. Therefore, the etching rates of PMMA are controlled mainly by diffusion of atomic oxygen in the CF_4/O_2 plasma.

Molecular Weight Distribution in the Cross Section of the Film

It seems reasonable that the species, e.g., atomic oxygen and radicals induced in the plasma, which relate to the decomposition of PMMA, have comparatively small molecular sizes, and therefore they easily permeate into the film. Hence, it presents the possibility that the polymer decomposition occurs not only at the film surface but also at deep layer of the film.

The molecular weight distribution in the cross section of the film has been estimated from the GPC data, which are obtained under the same conditions but at various initial film thicknesses.

TABLE II
Activation Energies for the Etching Rate of PMMA Calculated from Figures 8 and 9

O_2 (%)	rf power (W)	Activation energy (kcal/mole)
0	200	4.0
5	200	4.4
15	200	6.5
21	200	6.3
100	200	4.4
5	100	5.7
5	300	3.1
100	100	4.4

The experimental and calculation procedures are as follows. The film samples of p pieces on the wafer, which have different thicknesses, were etched at the same plasma etching conditions, and finally they give the thicknesses of δ_1, δ_2, ... δ_p ($\delta_1 > \delta_2 > -> \delta_p$) and their GPC peak heights to the standard molecular weights M_{w1}, M_{w2}, ... M_{wl} are expressed

$$\begin{matrix} h_{11}, h_{12}, \cdots h_{1l} \\ h_{21}, h_{22}, \cdots h_{2l} \\ \cdot \quad \cdot \quad \cdot \\ \cdot \quad \cdot \quad \cdot \\ \cdot \quad \cdot \quad \cdot \\ h_{p1}, h_{p2}, \cdots h_{pl} \end{matrix}$$

If it is assumed that the change of polymer density does not occur by etching, the new peak heights of the layer from δ_k to δ_{k+1} in depth is calculated to the standard molecular weights of M_{w1}, M_{w2}, ... M_{wl} by eq. (2). From these new peak heights, the weight average molecular weight $\overline{M}_{w(k,k+1)}$ for the layer from δ_k to δ_{k+1} in depth are obtained from eq. (3).

$$\begin{aligned} H_{(k,k+1),1} &= h_{k,1} \frac{\delta_k}{\sum_{n=1}^{l} h_{1m}} - h_{k+1,1} \frac{\delta_{k+1}}{\sum_{m=1}^{l} h_{2m}} \\ H_{(k,k+1),2} &= h_{k,2} \frac{\delta_k}{\sum_{m=1}^{l} h_{1m}} - h_{k+1,2} \frac{\delta k+1}{\sum_{m=1}^{l} h_{2m}} \\ &\vdots \qquad\qquad \vdots \qquad\qquad \vdots \\ H_{(k,k+1),l} &= h_{k,l} \frac{\delta_k}{\sum_{m=1}^{l} h_{1m}} - h_{k+1,l} \frac{\delta_{k+1}}{\sum_{m=1}^{l} h_{2m}} \end{aligned} \tag{2}$$

$$M_{w(k,k+1)} = \frac{\sum_{m=1}^{l} H_{(k,k+1),m} M_{wm}}{\sum_{m=1}^{l} H_{(k,k+1),m}} \tag{3}$$

Figure 13 shows the calculated results of $\overline{M}_w$ variation in the cross section with respect to the etching time, which are displayed to combine the values at average thickness.

It becomes apparent that the $\overline{M}_w$ decreasing ratio at the shallow layer is larger than that of the deep layer. In the layer from 3 to 4 μm in depth, the decomposition has occured after 5 min, because the $\overline{M}_w$ of the original PMMA is 6.1×10^5. Therefore, the species decomposed PMMA permeate into film with fairly high speed, and the PMMA decomposition occurs not only at the film surface but also in the deep layer of the film.

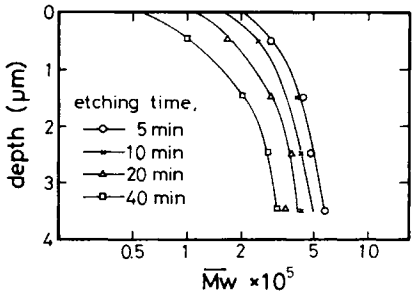

Fig. 13. PMMA molecular weight variations in the cross section of the film (PMMA-3; etching gas, CF_4/O_2 = 95/5; etching temperature, 60°C; rf power, 200 W).

CONCLUSION

It becomes clear that the major PMMA decomposition in CF_4/O_2 plasma etching proceeds on the mechanism of random chain scission because very small kinetic chain lengths are estimated from the GPC data. Atomic oxygen and radicals induced in the plasma seem to contribute mainly to random chain scission. Therefore the oxygen concentration exerts a huge influence on the PMMA durability as a resist.

The Arrhenius plots of PMMA for the plasma etching rate bend above about T_g increasing the etching rate rapidly where a remarkable pattern deformation is observed. It is important that, in practical plasma etching, the etching temperature is maintained below the bending point which falls apart from T_g according to increase of oxygen concentration.

Activation energy of the PMMA etching rate, which depends on oxygen concentration and rf power, indicates various values from 3.1 to 6.5 kcal/mole at linear part of the Arrhenius plots. Magnitude of these activation energies suggests diffusion control.

The results of the molecular weight variation in the cross section of the film suggest that the active species permeate into the film with fairly large speed and the PMMA decomposition occurs not only at the film surface but also in the deep layer of the film.

The author is grateful to Dr. S. Sugawara, S. Oikawa, and J. Shimada for their helpful discussions.

Reference

1. K. Harada, *J. Electrochem. Soc.*, **127** (2), 491 (1980).
2. R. G. Poulsen, *J. Vac. Sci. Technol.*, **14** (1), 266 (1977).
3. J. W. Coburn and H. F. Winters, *J. Vac. Sci. Technol.*, **16** (2), 391 (1979).
4. C. David, D. Fuld, and G. Geuskens, *Makromol. Chem.*, **139,** 269 (1970); **160,** 135 (1972); **160,** 347 (1972).
5. J. R. MacCallum and C. K. Schoff, *J. Chem. Soc. Faraday Trans.*, **67,** 2372 (1971).
6. A. Barlow, R. S. Lehrle, J. C. Robb, and D. Sunderland, *Polymer* (London), **8,** 537 (1967).
7. R. B. Fox, *Progress in Polymer Science, Vol. 1*, A. D. Jenkins, Ed., Pergamon, New York, 1967.
8. H. F. Winters, J. W. Coburn, and E. Kay, *J. Appl. Phys.*, **48,** 4973 (1977).
9. W. R. Harshbarger, R. A. Porter, T. A. Miller, and P. Norton, *Appl. Spectrosc.*, **31** (3), 201 (1977).
10. J. F. Battey, *J. Electrochem. Soc.*, **124** (1), 147 (1977).
11. M. Tsuda, S. Oikawa, S. Ohnogi, and A. Suzuki, *Proceeding on Micro Lithography*, R. P. Kramer, Ed., Delft University Press, Amsterdam, 1980.
12. A. Todd, *J. Polym. Sci.*, **42,** 223 (1960).
13. S. L. Madorsky, *Polym. Rev.*, **7,** 295 (1964).
14. H. H. G. Jellinek, *Aspects of Degradation and Stabilization of Polymers*, Elsevier Scientific, New York, 1978.
15. J. R. MacCallum and C. K. Schoff., *J. Chem. Soc. Faraday Trans.*, **67,** 2383 (1971).
16. G. Bagby, R. S. Lehrle, and J. C. Robb, *Makromol. Chem.*, **119,** 122 (1968).
17. Y. Yamamoto, M. Himei, and K. Hayashi, *Macromolecules*, **10,** 1316 (1977).
18. J. E. Gullet, *Pure Appl. Chem.*, **49,** 249 (1977).
19. C. J. Mogab, A. C. Adams, and D. L. Flamm, *J. Appl. Phys.*, **49** (7), 3796 (1978).

Received August 28, 1980
Accepted December 8, 1980